Simulation of contact line dynamics in a two-dimensional capillary tube by the lattice Boltzmann model

Lewen Fan, Haiping Fang, and Zhifang Lin
Research Center for Theoretical Physics, Fudan University, Shanghai 200433, China
(Received 23 August 2000; published 17 April 2001)

During immiscible-fluid displacement, the contact angle between the interface and the wall of a tube, as well as the velocity V of the contact line where a fluid interface intersects the wall of a tube, depends on the applied capillary pressure P_{cap}. In this paper, the contact line dynamics of immiscible-fluid displacement is simulated by using the lattice Boltzmann model in a two-dimensional capillary channel with an ideally smooth wall. The V dependence of the contact angle is studied for two different wetting cases. Our simulational results are in good agreement with those based on theoretical computations and with molecular dynamics simulations. In particular, the power-law behavior $P_{cap} \sim V^x$ is found with an exponent x very close to 1. The simulations suggest that the lattice Boltzmann model may serve as an alternative reliable quantitative approach to study the contact line dynamics, and also may be a promising tool for invesitgating some other immiscible displacement related subjects.

DOI: 10.1103/PhysRevE.63.051603 PACS number(s): 68.05.−n, 47.11.+j, 68.08.−p

I. INTRODUCTION

The displacement of fluid by another immiscible fluid involves a variety of interesting subjects that are of great relevance to a wide range of industrial processes like oil recovery and coating [1]. Among others, the contact line dynamics has attracted much attention over the past few decades [2–16] since the pioneering work by Dussan [2]. The dynamic behavior of a contact line, where a liquid-liquid or liquid-vapor interface intersects a solid wall, is governed by the dynamics of the three phases, adding considerably to the difficulty of the analysis, as well as to the academic interest. The motion of the interface, as well as the contact line formed by two immiscible fluids and a solid wall in a capillary tube, was investigated in many cases, such as complete or partial wetting of fluids to a solid wall, an ideally smooth wall surface, or a heterogeneous wall surface.

Macroscopically, some theories based on classical hydrodynamics were raised to reveal the dynamic behavior of the interface. Cox [5] used the method of matching asymptotic expansions to investigate the dynamics involved in the movement of a contact line while the solid surface is ideally smooth. Shikhmurzae [7] dealt with a general mathematical model which describes the motion of an interface between immiscible viscous fluids along a smooth homogeneous solid surface in the case of small capillary and Reynolds numbers. Jansons [4] considered the unsteady motion of a fluid-fluid interface above and attached to a solid surface with one-dimensional periodic roughness in the limit of small capillary number Ca.

Microscopically, some authors used molecular dynamics simulations to study the dynamic behavor of the interface and the contact line in immiscible fluids system. Koplik *et al.* [8] observed a breakdown of the no-slip condition, consistent with the theoretical predictions of Dussan [2], as well as a velocity-dependent advancing and receding contact angles. Simulations by Thompson and co-workers [9,10] also supported the breakdown of the no-slip condition. In particular, changes with capillary number in the interface shape and the dynamic contact angle were found to be quantitatively consistent with those predicted based on the macroscopic theory [5].

Macroscopic theories are usually applied to systems with relatively simple geometries. They generally encounter difficulty when dealing with complex and changeable geometries. On the other hand, although molecular dynamics simulations have the advantage of being faithful to the microscopic nature of the fluid, they are extremely computationally intensive. As an alternative numerical approach, the lattice Boltzmann (LB) method [17–20] has proved competitive in studying various types of fluid-related systems. It is ideally suited to investigate phenomena on a hydrodynamic length scale. In addition, when incorporated with appropriate boundary conditions (see, e.g., Refs. [21,22]), it provides a promising numerical tool to deal with systems of complex and flexible boundaries [22]. In this paper, by studying the behavior of the dynamic contact angle in a simple geometry quantitatively, we prove the LB method to be a reliable approach for the dynamics of the interface, contact line, and contact angle during the immiscible-fluid displacement procedure in capillary tube. We expect to find many applications in studying such subjects effectively in more complex geometries.

The simulations are performed on a two-dimensional (2D) channel, as shown in Fig. 1, so that a contact line becomes a contact point where the three phases intersect. Two kinds of fluids are put in the 2D channel lattice, with a pressure drop between two open ends. Two cases of different wetting conditions are considered. One is an ideal condition in which there is no interaction between the fluids and the wall, so that the static contact angle $\theta_0 = \pi/2$. The other case mimics a kind of real experimental case, in which one fluid that has an attractive interaction with the wall displaces an immiscible fluid that has a repulsive interaction with the wall. The latter case has a static contact angle $\theta_0 < \pi/2$. The relation curves of the contact angle θ vs the average velocity of the contact line are obtained for these two cases, respectively. The

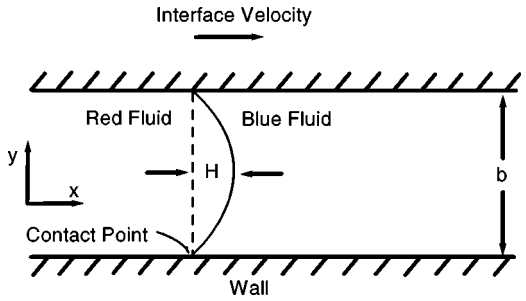

FIG. 1. The schematic diagram of the simulational framework.

curves agree excellently with the theoretical relations given by Cox *et al.* [5], and can be superimposed onto a single curve by a certain transformation using a scale function [13,14,23] with a single parameter K, implying the universal scaling behavior of the contact angle vs the contact line velocity. In particular, the power-law behavior $P_{cap} \sim V^x$ is found, with the exponent x very close to 1, in good agreement with the results based on the macroscopic theory and the molecular dynamics simulation [5,9,10].

This paper is organized as follows. In Sec. II, some basic ideas of the LB model are summarized, and a simulational framework is introduced. Numerically experimental data are analyzed, and results presented in Sec. III. A discussion on our simulations is finally given in Sec. IV.

II. MODEL AND THEORY

Let us first recall some basic ideas of the one-component lattice Boltzmann method [20]. The equation of evolution is given by 2D nine velocities model (D2Q9 model [20])

$$f_i(\mathbf{x}+\delta\mathbf{e}_i, t+\delta) - f_i(\mathbf{x},t) = -\frac{1}{\tau}[f_i(\mathbf{x},t) - f_i^{(0)}(\mathbf{x},t)],$$

$$i = 0,1,\ldots,8, \tag{1}$$

where $\mathbf{e}_0 = (0,0)$, $\mathbf{e}_i = [\cos[(i-1)/2]\pi,\ \sin[(i-1)/2]\pi]$ for $i = 1, 2, 3$, and 4, and $\mathbf{e}_i = [\cos[(2i-1)/4]\pi,\ \sin[(2i-1)/4]\pi]$ for $i = 5, 6, 7$, and 8 are nine discretized velocities that a particle can have. The distribution function $f_i(\mathbf{x},t)$ denotes the population for particles that move with a velocity $\mathbf{e}_i$ at a site $\mathbf{x}$ and time t, $f_i^{(0)}(\mathbf{x},t)$ is the corresponding equilibrium distribution function and τ is the relaxation time. It has been shown that if the equilibrium distribution function is chosen to be [20]

$$f_0^{(0)} = \alpha\rho - \frac{2}{3}\rho\mathbf{u}\cdot\mathbf{u},$$

$$f_i^{(0)} = \frac{(1-\alpha)\rho}{5} + \frac{1}{3}\rho(\mathbf{e}_i\cdot\mathbf{u}) + \frac{1}{2}\rho(\mathbf{e}_i\cdot\mathbf{u})^2 - \frac{1}{6}\rho\mathbf{u}\cdot\mathbf{u}$$

$$\text{for } i = 1,\ldots,4, \tag{2}$$

$$f_i^{(0)} = \frac{(1-\alpha)\rho}{20} + \frac{1}{12}\rho(\mathbf{e}_i\cdot\mathbf{u}) + \frac{1}{8}\rho(\mathbf{e}_i\cdot\mathbf{u})^2 - \frac{1}{24}\rho\mathbf{u}\cdot\mathbf{u}$$

$$\text{for } i = 5,\ldots,8,$$

at the long-wavelength limit, the Navier-Stokes equations with an equation of state $p = c_s^2\rho$ can be recovered from the kinetic equation (1). Here $c_s = 1/\sqrt{3}$ is a constant sound speed, and the parameter α in Eq. (2) is usually chosen as 4/9 in the D2Q9 model [20]. The fluid density and velocity are defined by

$$\rho = \sum_{i=0}^{8} f_i, \quad \rho\mathbf{u} = \sum_{i=1}^{8} f_i\mathbf{e}_i. \tag{3}$$

As usual, for immiscible-fluid displacement, we use the colors blue and red to distinguish two immiscible fluid components. There are currently three LB methods developed for the study of multiphase and/or multicomponent flow. They are the recolor scheme [24], the potential model [25,26], and the free energy approach [27,28]. In this paper we use the potential model, partly as it is very convenient for considering the different wetting cases. The details of the potential model theory for a two-component fluid are available in Refs. [25,26]. The following is a brief description of the entire algorithm based on Shan and co-workers model [25,26].

It can be assumed that there exists an initial $f_{i,k}(\mathbf{x},t)$ over the entire lattice at a time t, where the subscript k is an index denoting a fluid component. The density $\rho_k(\mathbf{x},t)$ and velocity $\mathbf{u}_k(\mathbf{x},t)$ at $\mathbf{x}$ are obtained from $f_{i,k}(\mathbf{x},t)$ by the following equations:

$$\rho_k = \sum_i f_{i,k}, \qquad \rho_k\mathbf{u}_k = \sum_i f_{i,k}\mathbf{e}_i. \tag{4}$$

The equilibrium velocity $\mathbf{u}_k^{(eq)}$ is then given by

$$\rho_k\mathbf{u}_k^{(eq)} = \rho_k\mathbf{u}' + \tau_k\mathbf{F}_k, \tag{5}$$

where $\mathbf{F}_k$ is the total interparticle force acting on a component k at a site $\mathbf{x}$,

$$\mathbf{F}_k(\mathbf{x}) = -\psi_k(\mathbf{x})\sum_{\mathbf{x}'}\sum_{k'} G_{k,k'}(\mathbf{x},\mathbf{x}')\psi_{k'}(\mathbf{x}')(\mathbf{x}'-\mathbf{x}), \tag{6}$$

and $\mathbf{u}'$ is a common average velocity given by the equation

$$\mathbf{u}' = \left(\sum_k \frac{\rho_k\mathbf{u}_k}{\tau_k}\right) \Big/ \left(\sum_k \frac{\rho_k}{\tau_k}\right). \tag{7}$$

The Green's function $G_{k,k'}(\mathbf{x},\mathbf{x}')$ satisfies $G_{k,k'} = G_{k',k}$, and $\psi_k(\mathbf{x}) = \psi_k[\rho_k(\mathbf{x})]$ is a function of the density $\rho_k(\mathbf{x})$. It is assumed that $\psi_k[\rho_k(\mathbf{x})] = \rho_k(\mathbf{x})$ for simplicity [25,26]. Usually it is sufficient to involve only nearest-neighbor homoge-

neous isotropic interactions, so that $G_{k,k'}(\mathbf{x},\mathbf{x}')$ can be reduced to the following symmetric matrix with constant elements:

$$G_{k,k'}=\begin{cases}0, & |\mathbf{x}-\mathbf{x}'|>c\\ g_{k,k'}, & |\mathbf{x}-\mathbf{x}'|\leqslant c.\end{cases} \tag{8}$$

Here c is the lattice spacing (we take $c=1$), and $g_{k,k'}$ is a parameter that characterizes the strength of the interaction potential. In our simulations, we choose $g_{k,k'}=0.5$ for the interaction between the two immiscible fluid components and, for simplicity, we set the relaxation time $\tau_k=1$ for both components. Too large a value of $g_{k,k'}$ may likely produce a negative distribution function, resulting in a numerical instability, while a small value of $g_{k,k'}$ is not effective in producing the desired separation of the fluids. A more detailed discussion of the choice of the values of $g_{k,k'}$ and τ_k can be found in Ref. [29].

Our simulations are carried out on a 1000×20 two-dimensional channel lattice, as shown schematically in Fig. 1. Referring to Ref. [16], we compare the size of the lattice to that of the real experimental framework. If 20 lattice unit spacings (LUS's) are equal to 1 mm (Kumar and co-workers used Pyrex tubes of radius $R=0.5$ mm), one has the following correspondence: one LUS is equal to 0.05 mm, and 1 sec$=2.97\times10^5$ steps. As a result, our simulational framework does not relate to microscopic scale (molecular scale).

The pressure difference between two ends of the plane channel is denoted by $\Delta P=P_1-P_2$, where P_1 and P_2 are pressures at the left and right ends, respectively. It is supposed that the red fluid displaces the blue one from the left-hand end (inlet) to the right-hand end (outlet). Bounce back boundary conditions are adopted on the upper and lower solid walls, in which the fluid particles simply bounce backward according to their directions before their collision with the solid wall. The inlet-outlet pressure and velocity flow boundary conditions supposed by Zou and He [30] are applied on the two open ends of the plane channel. In order to simulate the natural wetting conditions in a real experiment, we lay a fixed layer of yellow fluid particles on the wall with a certain constant density, and introduce two parameters $g_{b,y}$ and $g_{r,y}$ to control the interations between the wall blue component and wall red component, respectively. In the simulation, the absolute values of $g_{b,y}$ and $g_{r,y}$ are chosen to be identical for simplicity. One can choose different absolute values for $g_{b,y}$ and $g_{r,y}$. However, the effect is essentially the same. It serves only to produce a different wetting case in the context of the present work, provided that the values of $g_{b,y}$ and $g_{r,y}$ are small as compared with $g_{r,b}$, the magnitude for the repulsive interaction between the red and blue fluid components.

When the simulation begins, fluid particles on all lattice sites are assumed to be blue. The inlet-outlet pressure-velocity boundary conditions are therefore applied for blue fluid. All blue fluid particles which are on the left side of a certain x position, including the inlet, will be repainted red after enough time steps have passed to make sure the flow over the entire lattice is stable. The procedure of repainting may cause some unphysical transient states on the field of flow for a certain time that is rather short relative to the entire simulational time duration. Measurement is done when the interface of the two fluids creeps near the center position of the channel to reduce boundary effects.

According to the analytical solution of Poiseuille flow in a plane channel driven by pressure difference, the pressure drop P_1-P_2 can be expressed as a sum of two parts,

$$P_1-P_2=P_{cap}+\frac{12\mu LV}{b^2}, \tag{9}$$

where b denotes the width of the plane channel, L is the length of a capillary tube between the places where P_1 and P_2 are measured, and P_{cap} denotes the pressure drop arising from the interface. The second term on the right hand side of Eq. (9) is the pressure drop caused by viscous dissipation. In a plane channel of width b and at low velocity, P_{cap} is directly related to the cosine of the contact angle θ by [13,14]

$$P_{cap}=\frac{2\gamma}{b}\cos\theta. \tag{10}$$

In our simulation, the dimensionless interface velocity Ca is employed to take the place of the contact line velocity V, where $\mathrm{Ca}\equiv\mu V/\gamma$, with γ being the interfacial tension of the fluid interface, and μ the mean viscosity of the two fluids. The viscosity for component k is related to the relaxation time by $\mu_k=(2\tau_k-1)/6$, as measured in lattics units. The interfacial tension γ is obtained by another series of simulational experiments. We performed the LB simulation on a 200×200 plane lattice to do a series of bubble tests [31] with a series of varied radii R. The interfacial tension γ was found to be $\gamma=0.172(3)$ for the present simulation parameters by the Laplace law $P_{in}-P_{out}=\gamma/R$.

It can be imaged that, as the flow velocity increases, the interface is incrementally deformed to the right. The contact angle varies continuously as the velocity of the interface increases from a macroscopic viewpoint. The deformed interface is therefore measured by the contact angle (also referred as the apparent contact angle) [14]

$$\theta=\arctan\left[\frac{1-h^2}{h}\right], \tag{11}$$

where $h=H/b$, with H being the distance from the center point of the interface to the contact point on the wall along the x direction (see Fig. 1).

Theoretically, Cox used the method of matching asymptotic expansions and the scaling function found by Hoffman [23],

$$g(\theta)=g[\theta_0(0)]+\mathrm{Ca}\ln(k/l_s), \tag{12}$$

to predict the scaling behavior of θ vs Ca [5]. As the slipping length $l_s=l_d/\mathrm{Ca}$ for Jansons' picture [4], with l_d being the roughness of the wall, Eq. (12) becomes

$$g(\theta)=g[\theta_0(0)]+\mathrm{Ca}\ln(k/l_d)+\mathrm{Ca}\ln\mathrm{Ca}, \tag{13}$$

where k is a model-dependent parameter and $\theta_0(0)$ is the static contact angle. The function $g(\theta)$ is given by (see Ref. [14])

$$g(\theta)=\int_0^{\theta} d\varphi[f(\varphi)]^{-1},$$

$$f(\varphi)=\frac{2\sin\varphi\{q^2(\varphi^2-\sin^2\varphi)+2q[\varphi(\pi-\varphi)]+(\pi-\varphi)^2-\sin^2\varphi\}}{q(\varphi^2-\sin^2\varphi)[(\pi-\varphi)+\sin\varphi\cos\varphi]+(\varphi-\sin\varphi\cos\varphi)[(\pi-\varphi)^2-\sin^2\varphi]}, \tag{14}$$

where $q=\mu_2/\mu_1$. With the specified wetting condition, one has $\theta_0(0)$. By choosing a suitable parameter $K=\ln(k/l_d)$, one can next obtain θ as the function of Ca based on Eqs. (13) and (14). Although the value of $\theta_0(0)$ will be different in different wetting cases, the value of $K=\ln(k/l_d)$ should remain the same for different wettings. The universal scaling law [Eq. (13)], with K independent of the wetting condition, therefore provides a first check of the simulation results.

III. RESULTS ANALYSIS

It is supposed that the red fluid displaces the blue one from left to right. The pressure on all the lattice sites on the right open end is set constant, while that on the inlet varies, to achieve different values of Ca using the boundary conditions suggested by Zou and He [30]. With the pressure difference between the inlet and outlet, the interface moves at a nearly constant velocity with slightly undulant h when the flow becomes steady. We then can measure the time average velocity of the interface at the center of the channel. Note that the average velocity of the interface is equal to that of the contact line when the flow becomes steady. Also in this region, $\overline{h}$ (the time average of h) is measured to obtain θ based on Eq. (11). Thus the relation θ vs Ca is obtained. Figure 2 shows the relation of θ vs $\log$ Ca for two different wetting cases. The diamonds on the upper curve are simulational results for the wetting case 1, in which two fluids have the same vanishing interaction with the solid wall and thus the static contact angle $\theta_0=\pi/2$. The triangles on the lower curve are those for the wetting case 2, in which $g_{b,y}=-g_{r,y}=0.01$ so that $\theta_0<\pi/2$. The two solid curves are the theoretical curves based on Eqs. (13) and (14) with different $\theta_0(0)$ and identical $K=\ln(k/l_d)=21.8$. Note that, in the present case, $q=1$, and thus $f(\varphi)$ in Eq. (14) reduces to

$$f(\varphi)=\frac{2\pi\sin\varphi}{\pi\varphi-\varphi^2-\sin\varphi(\sin\varphi+\pi\cos\varphi-2\varphi\cos\varphi)}.$$

It is seen from Fig. 2 that the simulation results are in excellent consistency with the theoretical predictions. The two solid curves fit the simulation data well, with a single param-

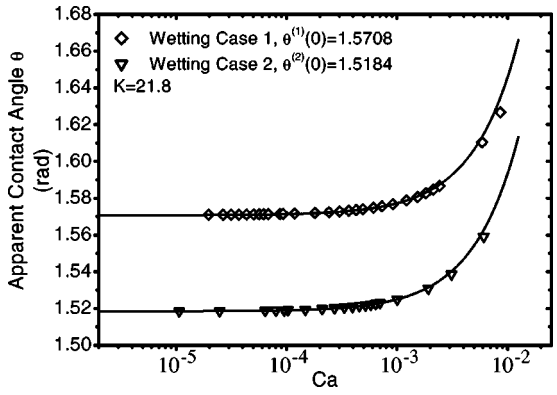

FIG. 2. Apparent contact angle plotted as a function of Ca for two different wetting cases, $\theta^{(1)}(0)=\pi/2$ and $\theta^{(2)}(0)<\pi/2$. The solid lines are the fits produced by using Eqs. (13) and (14), with $K=21.8$.

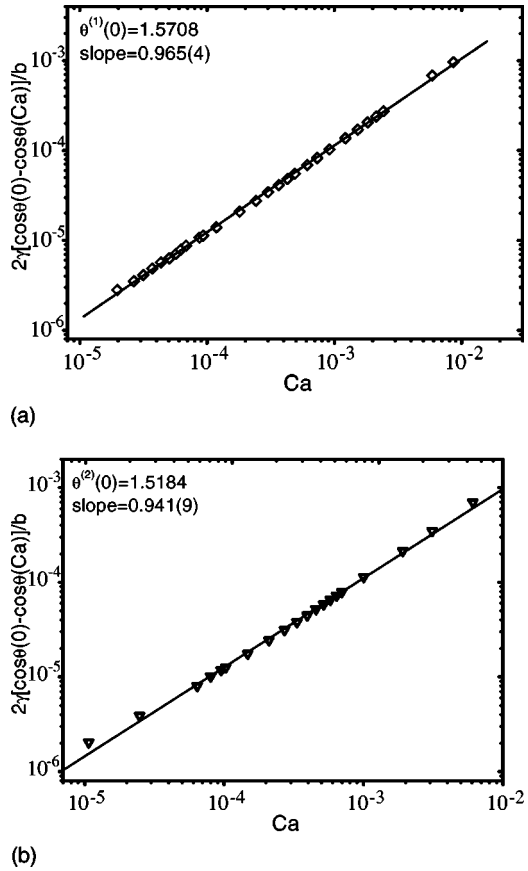

FIG. 3. P_{cap} as a function of Ca for two wetting cases. Power law $2\gamma[\cos\theta(0)-\cos\theta(\mathrm{Ca})]/b\sim \mathrm{Ca}^x$ is manifest in both cases: (a) $\theta^{(1)}(0)=1.5708$ and $x=0.965(4)$, (b) $\theta^{(2)}(0)=1.5184$ and $x=0.941(9)$.

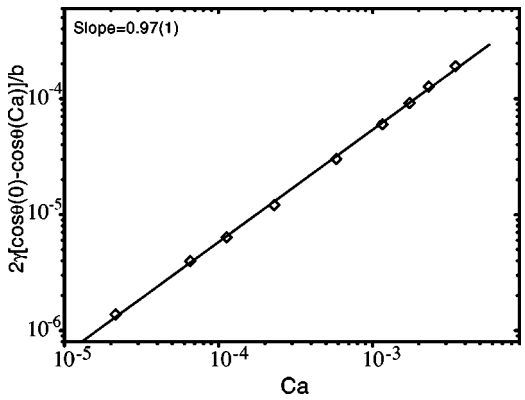

FIG. 4. Power law $2\gamma[\cos\theta(0)-\cos\theta(\mathrm{Ca})]/b \sim \mathrm{Ca}^x$ obtained on a 2000×40 lattice with $\theta(0)=1.5708$ and $x=0.97(1)$. Note that the value of x is greater than in Fig. 3, suggesting that x will be closer to unity and the discretization effect will decrease if the underlying lattice is refined.

eter $K=21.8$ for different wetting cases and different static contact angle θ_0, which implies that the two curves obey the universal scaling behavior, although they have different values of $\theta_0(0)$. By a suitable transfer on the lower curve, two curves can be superimposed upon each other through a uniform additive shift horizontally along the Ca axis (see, e.g., Ref. [14]).

Referring to Eq. (10), the relation between P_{cap} and Ca can be obtained by the relation of $(2\gamma/b)[\cos\theta(0)-\cos\theta]$ vs Ca [14]. Figure 3 shows the scaling behavior of $(2\gamma/b)[\cos\theta(0)-\cos\theta]\sim \mathrm{Ca}^x$, with x very close to 1. The exponent is found to be $x=0.965(4)$ for wetting case 1 [Fig. 3(a)], and $x=0.941(9)$ for wetting case 2 [Fig. 3(b)]. Except for a few data points for which the values for Ca fall close to 10^{-5}, all data of these two wetting cases are excellently linearly fit. These results agree with the theory that x will be exactly 1 if the wall surface is ideally smooth, i.e., P_{cap} will be linearly proportional to Ca.

When Ca is small, some data points in Fig. 3 seems go above the linear-fit line. The discretization effect of the lattice manifests itself here. The current model is for an ideally smooth wall. However, in the LB method, the position of the interface is usually determined by an interpolation of the densities of neighbor sites. So, when Ca is small enough, the discretization of the lattice may affect the simulation like some type of periodic heterogeneity on the wall surface. Because the lattice unit spacing in our simulations is on a macroscopic scale, such a likeness is believed to correspond to the smooth periodic heterogeneity on the wall surface.

If the lattice is refined, the discretizing effect may be reduced, and the exponent x turns out to be closer to unity. This is confirmed by some simulations for both wetting cases on a refined lattice. The result for wetting case 1 on a lattice of 2000×40 is presented as an example in Fig. 4. The slope 0.97(1) of the linear fit is clearly greater than that based on a 1000×20 lattice suggesting that the exponent x may approach unity if the discretizing effect is eliminated in the LB simulation.

It should be noted that present simulations produce the dimensionless velocity Ca of the interface in a range from 10^{-5} to 10^{-2}, and that the corresponding value of θ varies in a rather limited region. In Fig. 4 of Ref. [14], the largest value of θ approaches π, which requires a self-consistent iteration procedure to obtain $\theta(\mathrm{Ca})$ [14]. However, due to the limited value range of the contact angle θ in the present simulation, there is no need to perform a self-consistent iteration as in Ref. [14]. In fact, Eqs. (13) and (14) fit our data well enough, with a single value of $K=21.8$, and two different constants $\theta_0^{(1)}=\pi/2$ and $\theta_0^{(2)}<\pi/2$.

IV. DISCUSSION

In this paper, we have focused on the velocity dependence of the cosine of the contact angle θ in a 2D capillary tube with homogeneous wall surface. Macroscopic theory [5] and molecular dynamic simulations [9,10] both indicated a power law scaling behavior with the exponent $x=1$ for a partially wetting fluid on this kind of wall surface. Our simulation results agree excellently with their conclusions. The linear fits in Figs. 3 and 4 show that x verges on 1 for ideally smooth boundaries. It is believed that x will be smaller than 1 if some kind of heterogeneity, such as periodic roughness, is introduced into the wall in simulations. In fact, some data of low Ca in Fig. 3 suggest evidence for this belief.

Several authors considered theoretically and experimentally how heterogeneity on wall a surface affects the power law scaling behavior of $\cos\theta$ vs Ca. Theoretical models produced a range of values for the power law exponent x. Joanny and Robbins considered the case of a contact line moving past periodic heterogeneities at a constant velocity, and obtained a result of $x=2/3$ for smooth defects on a wall surface [12]. For the case of discontinuous defects they found $x=1$, just as in the case of an ideally smooth wall surface. Raphael and de Gennes independently derived $x=2/3$ for smooth defects such as dilute concentrations [6]. Functional renormalization group calculations by Ertaş and Kardar yielded $x=9/7$ from an expansion around the mean field solution for discontinuous defects [15]. Sheng and Zhou predicted $0<x\leqslant0.5$ by considering a capillary wave dissipation mechanism [13,14]. Experiments also reported a variety of exponents. The experiment of Stokes *et al.*, with a glycerol-menthanol solution and mineral oil, found that $x=0.40(5)$ [11]. Capillary rise experiments showed $x=0.5$ for a glyecrol-water solution with alkanes as well as for a glycerol-water solution with silicone oils [32]. Kumar *et al.* found $x=0.20(3)$ for water-alkane interfaces [16].

Our simulations suggest that the LB model may be a reliable numerical technique for studying immiscible-fluid displacement related subjects, such as the dynamics of the interface, the contact line, and the contact angle. In particular, when incorporated with appropriate boundary conditions, the LB model may serve as an effective numerical tool to study such subjects for systems with complex geometry, where the macroscopic theory may encounter some difficulty and the molecular dynamics approach may turn out to be too computationally intensive. Further investigation would be of interest in an attempt to clarify the somewhat conflicting results regarding the value of the power law exponent x in the

case when some kinds of heterogeneity are introduced into the wall surface. We are currently in the process of this investigation. Some qualitative results on a sinusoidal tube have in fact been obtained, and will be published elsewhere [33].

ACKNOWLEDGMENTS

The work was supported by NSF of China through Grant No. 19704003. Z. L. was also supported by Climbing Project and NSFC 19834070.

[1] P.G. de Gennes, Rev. Mod. Phys. **57**, 827 (1985).
[2] E.B. Dussan, AIChE J. **23**, 131 (1977); Annu. Rev. Fluid Mech. **11**, 371 (1979).
[3] L.M. Hocking, J. Fluid Mech. **76**, 801 (1976); **79**, 209 (1977).
[4] K.M. Jansons, J. Fluid Mech. **154**, 1 (1985); **167**, 393 (1986).
[5] R.G. Cox, J. Fluid Mech. **168**, 169 (1986).
[6] E. Raphaël and P.G. de Gennes, J. Chem. Phys. **90**, 7577 (1989).
[7] Y.D. Shikhmurzaev, J. Fluid Mech. **334**, 211 (1997).
[8] J. Koplik, J.R. Banavar, and J.F. Willemsen, Phys. Rev. Lett. **60**, 1282 (1988); Phys. Fluids A **1**, 781 (1989).
[9] P.A. Thompson and M. Robbins, Phys. Rev. Lett. **63**, 766 (1989).
[10] P.A. Thompson, W.B. Brinkerhoff, and M.O. Robbins, J. Adhes. Sci. Technol. **7**, 535 (1993).
[11] J.P. Stokes, M.J. Higgins, A.P. Kushnick, S. Bhattacharya, and M.O. Robbins, Phys. Rev. Lett. **65**, 1885 (1990).
[12] J.F. Joanny and M.O. Robbins, J. Chem. Phys. **92**, 3206 (1990).
[13] M. Zhou and P. Sheng, Phys. Rev. Lett. **64**, 882 (1990).
[14] P. Sheng and M. Zhou, Phys. Rev. A **45**, 5694 (1992).
[15] D. Ertaş and M. Kardar, Phys. Rev. E **49**, R2532 (1994).
[16] S. Kumar, D.H. Reich, and M.O. Robbins, Phys. Rev. E **52**, R5776 (1995).
[17] G.R. McNamara and G. Zanetti, Phys. Rev. Lett. **61**, 2332 (1988).
[18] F.J. Higuera and S. Succi, Europhys. Lett. **8**, 517 (1989).
[19] F.J. Higuera and J. Jimenez, Europhys. Lett. **9**, 663 (1989).
[20] Y.H. Qian, D. d'Humières, and P. Lallemand, Europhys. Lett. **17**, 479 (1992).
[21] R. Mei, L. Luo, and W. Shyy, J. Comput. Phys. **155**, 307 (1999).
[22] H. Fang, Z. Lin, and Z. Wang, Phys. Rev. E **57**, R25 (1998).
[23] R.L. Hoffman, J. Colloid Interface Sci. **50**, 228 (1975).
[24] A.K. Gunstensen, D.H. Rothman, S. Zaleski, and G. Zanetti, Phys. Rev. A **43**, 4320 (1991).
[25] X. Shan and H. Chen, Phys. Rev. E **47**, 1815 (1993); **49**, 2941 (1994).
[26] X. Shan and G. Doolen, J. Stat. Phys. **81**, 379 (1995); Phys. Rev. E **54**, 3614 (1996).
[27] M.R. Swift, S.E. Orlandini, W.R. Orsborn, and J.M. Yeomans, Phys. Rev. E **54**, 5041 (1996).
[28] A. Lamura, G. Gonnella, and J.M. Yeoman, Europhys. Lett. **45**, 314 (1999).
[29] H. Fang, R. Wan, and L. Fan, Chin. Phys. **9**, 515 (2000).
[30] Q. Zou and X. He, Phys. Fluids **9**, 6 (1997).
[31] S. Hou, X. Shan, Q. Zou, G. Doolen, and W.E. Soll, J. Comput. Phys. **138**, 695 (1997).
[32] T.A. Mumley, C.J. Radke, and M.C. Williams, J. Colloid Interface Sci. **109**, 413 (1986).
[33] H. Fang, L. Fan, Z. Wang, Z. Lin, and Y.-H. Qian, Int. J. Mod. Phys. B (to be published).